# Microscopic Internal Stress Generated via Martensitic Transformation in As-quenched Martensitic Steels

Daisuke Fukui[1], Ryota Nagashima[2], and Nobuo Nakada[*2]

[1]*Former Graduate Student, School of Materials and Chemical Technology, Tokyo Institute of Technology, Kanagawa 226-8503, Japan (Now at Japan Ground Seif-Defense Force)*
[2] *School of Materials and Chemical Technology, Tokyo Institute of Technology, Kanagawa 226-8503, Japan*

To further understand the internal residual stress that is microscopically generated via martensitic transformation in steels, the origin of internal strain attributed to Bain correspondence between face-centered cubic (fcc) and body-centered cubic (bcc) was evaluated from macro- and micro-viewpoints and its effect on hardness was investigated in martensitic steels, especially an interstitial free Fe-16%Ni martensite. Neutron diffractometry and electron backscatter diffraction analysis showed that body-centered cubic (bcc) crystal structure of as- quenched martensite contained elastic distortions leading to small tetragonality, even in martensitic steels without solute carbon, and that the extended [001] bcc of martensite tended to be parallel to < 001 > fcc of prior fcc austenite. In addition, the combination of micro-scale focused ion beam (FIB) and high precision digital image correlation techniques revealed that a micropillar fabricated by FIB processing within a martensite block was anisotropically deformed by the release of the residual strain distributed in as-quenched martensite in correspondence with the tetragonal distortions of the bcc crystal structure. These results prove that a small part of the Bain strain remained as an internal elastic residual strain and was microscopically distributed among Bain groups in lath martensite after martensitic transformation. Furthermore, the residual strain generated a hydrostatic internal stress, and therefore, the nanohardness decreased considerably by the micropillar fabrication accompanied by the release of the internal stress. This means that the internal residual stress in martensite among Bain groups influences the mechanical properties of martensitic steel. In the presentation, we will furthermore discuss the microscopic internal stress in steels with solute carbon.

***Keywords:*** *martensitic transformation, Bain correspondence, residual strains, micromechanics, internal stresses*

## 1. introduction

Martensite in steels is a very important transformation microstructure because it is used as the matrix of advanced high-strength steels. Lattice deformation of martensitic transformation in steels can be understood based on the Bain correspondence between face-centered cubic (fcc) and body-centered cubic (bcc) crystal structures, $(001)_{fcc}$ // $(001)_{bcc}$, $[010]_{fcc}$ // $[-110]_{bcc}$, where interstitial carbon atoms randomly distributed in the parent fcc austenite lattice become ordered in the bcc martensite lattice, leading to lattice expansion along the *c*-axis of bcc (increase in tetragonality). Recently, Maruyama et al.[1)] carefully evaluated the solute carbon content in as-quenched martensite using atom probe tomography while taking into account the autotempering phenomenon. They pointed out that martensite has a larger carbon solubility than bcc ferrite, and they proposed that the tetragonality of martensite is related to the microscopic strain distributed in martensite. Considering that Bain correspondence is realized upon martensitic transformation in steels regardless of the presence of solute carbon, it may be expected that the microscopic residual strain attributed to Bain strain remains, even in solute carbon-free martensite.

In this study, to understand the relationship between crystal structure and internal residual strain in martensite originating from Bain correspondence, the tetragonality of as-quenched martensite was investigated in an interstitial-free (IF) Fe–Ni martensite. A strain release test using micro-scale FIB and high-precision DIC techniques[2)] was carried out, and the tetragonality of martensite was macroscopically and microscopically evaluated by neutron diffractometry and electron backscatter diffraction (EBSD) analysis, respectively. Furthermore, the change in nanohardness due to the release of residual strain was investigated, and the effect of the internal residual stress of martensite on the mechanical properties was discussed.

## 2. Experimental Procedure

An Fe–16mass%Ni alloy was used in this study, where a small amount of Ti was added to eliminate the interstitial solute carbon and nitrogen (IF martensite). This alloy was austenitized at 1373 K for 1.8 ks, followed by water quenching to obtain fully lath martensite without retained austenite. The microstructure was observed using scanning electron microscopy (SEM: JSM-7001F, JEOL Ltd.) equipped with an electron backscatter diffractometer (EBSD). For the EBSD microscopic analysis, the acceleration voltage and step size were set to 15 kV and 100 nm, respectively. The obtained EBSD pattern was indexed by the OIM Data Collection ver. 7.1.0. and then analyzed using the OIM Analysis ver. 7.3.0. software developed by TSL Solutions. The microfabrication of each sample was performed using a field emission-type SEM with a focused ion beam system (FIB/FE-SEM: Scios, developed by FEI Japan Ltd.) and employing a current of 1.0 nA at a voltage of 30 kV so as to set the processing depth in one repetitive operation to be 0.5 μm. A cylindrical micropillar 10 μm in diameter was fabricated within a block of lath martensite until a total depth of 5.0 μm was reached. An SEM image with a resolution of 1536 × 1024 pixels was captured before and after FIB processing, and two-dimensional strain on the top surface of the cylindrical micropillar was measured accurately using DIC with the GOM Correlate Professional software developed by GOM. In the DIC analysis, the subsets were set to be squares of 148 × 148 pixels (~ 2.5 × 2.5 μm), and the step parameter was 10 pixels (170 nm).

## 3. Results and Discussion

### 3.1 Crystallographic features of as-quenched martensite

**Fig. 1** shows the crystallographic features of the as-

quenched IF martensite formed within a prior austenite grain. The martensite was analyzed using EBSD as being bcc-phase martensite. The ring indicated by the white arrow is the trace of the FIB processing. The as-quenched material was a typical lath martensite with a hierarchical substructure consisting of packets and blocks, and the relatively coarse blocks were well developed [Fig. 1(a)]. The $<001>_{bcc}$ pole figure of the martensite [Fig. 1(b)] exhibited a specific pattern that revealed a Kurdjumov-Sachs (K-S) orientation relationship with the prior austenite, $(111)_{fcc}$ // $(011)_{bcc}$, $[01\text{-}1]_{fcc}$ // $[1\text{-}11]_{bcc}$. Therefore, $<001>_{fcc}$ poles of the prior austenite could be expected based on the orientation relationship; these poles are indicated by the red, green, and blue circles in Fig. 1(b). Then, the martensite orientations were classified into three Bain groups that roughly shared the same Bain axis with the prior austenite, $<001>_{fcc}$ // $<001>_{bcc}$. The individual groups are colored red, green, and blue, respectively, in the Bain map shown in Fig. 1(c). The map reveals that the three Bain groups developed in a complex manner and that the area fractions of the groups were almost the same.

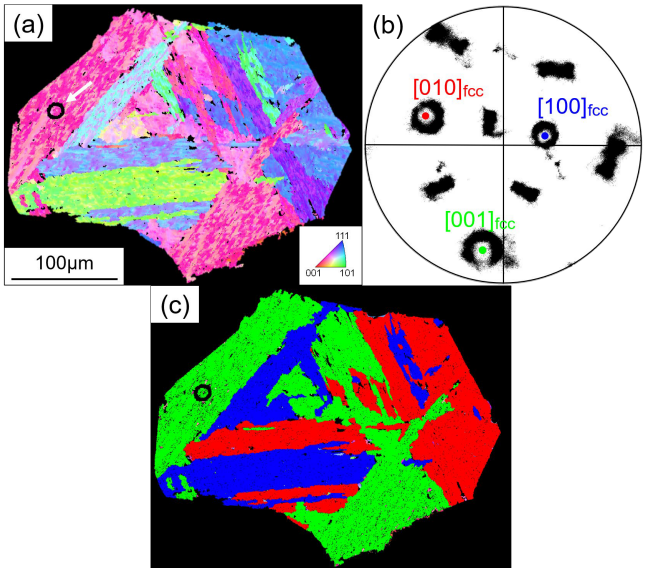


**Fig. 1**. The EBSD result of crystal orientation analysis for martensite formed within a prior austenite. (a) Invers pole figure map, (b) $<001>_{bcc}$ pole figure, and (c) Bain map for bcc-martensite.

### 3.2 Relation between microscopic strain and Bain strain

As shown in Fig. 1(a), a cylindrical micropillar was fabricated by FIB processing within one martensite block in another prior austenite grain. The processing depth increased with increasing FIB processing, and consequently, a cylindrical micropillar with a diameter of 10 μm was fabricated [see **Figs. 2**(a)–(d)]. Sags were formed by the processing at the edge of the top surface, but the area was relatively narrow. As a result, the irregular corrosion patterns previously formed by the chemical etching were maintained in the center of the top surface even after the FIB processing, which enabled the application of DIC analysis. The $<001>_{bcc}$ pole figure of the martensite within the targeted prior austenite grain is shown in Fig. 2(e). In addition, the $<001>_{bcc}$ poles of the martensite in the micropillar and the prior austenite expected under the K-S relationship are indicated by red and blue circles, respectively. In this figure, the crystal orientations of bcc and fcc were indexed on the basis of Bain correspondence. Here, we selected the analytical area such that $[010]_{bcc}$ was nearly parallel to the normal direction of the observation surface, and $[100]_{bcc}$ and $[001]_{bcc}$ existed in that area.

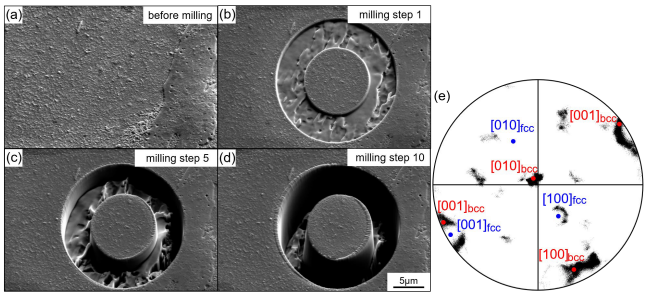


**Fig. 2**. SEM images (a-e) showing the fabrication of a micro-pillar by FIB processing. (e) $<001>_{bcc}$ pole figure of the martensite being the micro-pillar.

The in-plane strain on the top surface released by FIB processing is shown in **Fig. 3**. Two principal strains, $e_{p1}$ [Fig. 3(a)] and $e_{p3}$ [Fig. 3(b)] ($e_{p1} > e_{p3}$), at each subset were analyzed by DIC, and their directions were overlapped on the SEM image by red and blue arrows, respectively. Additionally, the pole figure showing the crystal orientation of martensite in the micropillar is shown in Fig. 3(c). It is confirmed in the strain distribution maps that $e_{p1}$ and $e_{p3}$ tended to be oriented in identical directions, as indicated by the white bidirectional arrows, although the data seemed to be scattered at the edge due to the formation of sags. This result suggests that a certain amount of residual strain existed in the martensite, as reported by Archie et al.[3], and that the residual strain was uniformly distributed in an identical direction within the martensite Bain unit.

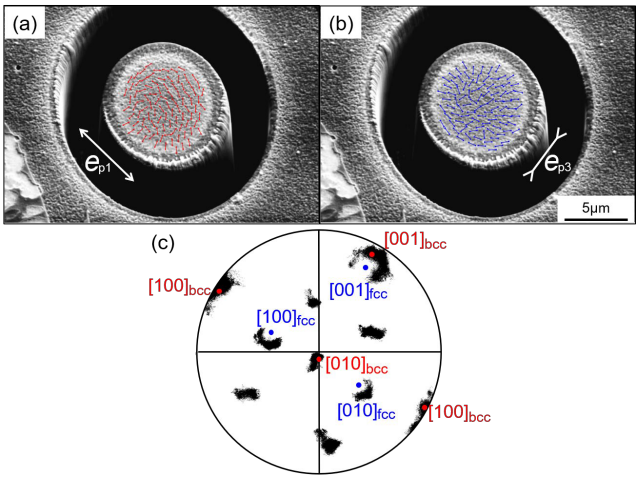


**Fig. 3**. The results of DIC analysis showing the strain released by the FIB processing. (a, b) shows the directions of two principal strains at individual analytical points on the top surface of the micro-pillar with SEM image. (c) is $<001>_{bcc}$ pole figure indicating the orientation of Bain correspondence in the micro-pillar.

In order to analyze the residual strain in relation to the crystal orientation of the martensite, the averaged strain

tensor was carefully evaluated by the coordinate rotation about the plane-normal direction every 15°. The averaged strain was measured by the displacement of a straight line which is parallel to the rotated coordinate axes and pass through a central point of the top surface. The mean in-plane strain was then summarized as the shape change of the circular rounded top surface, as shown in **Fig. 4**(a). According to the results of the crystal orientation analysis shown in Fig. 1(c), the corresponding crystal coordinate system of austenite under Bain correspondence, $x_1 = [1\text{-}10]_{fcc}$, $x_2 = [110]_{fcc}$, $x_3 = [001]_{fcc}$, are displayed in this figure. After the in-plane strain analysis [Fig. 4(a)], the two principal strains were measured to be $e_{p1} = 0.18\%$ and $e_{p3} = -0.24\%$, and they were gradually released by the FIB processing, as shown in **Fig. 4**(b). Comparing the in-plane strain with the crystal coordination system of austenite, it is understood that the directions of $e_{p1}$ and $e_{p3}$ were nearly parallel to $[1\text{-}10]_{fcc}$ and $[001]_{fcc}$, respectively. After similar analysis of Figs. 2-4 with respect to the other four martensite blocks, the same trend was confirmed every time, and it was found that the normal strain in $x_2$ was almost the same as that in $x_1$. That is, the residual strain in martensite, $e_{ij}^*$, is described in the crystal coordination system of austenite under Bain correspondence by the following tensor:

$$e_{ij}^* = \begin{pmatrix} -0.0018 & 0 & 0 \\ 0 & -0.0018 & 0 \\ 0 & 0 & 0.0024 \end{pmatrix} \quad \cdots\cdots[1]$$

The fact that the style of the residual strain corresponds to that of Bain strain, $e_{11}^* = e_{22}^*$ and $e_{11}^* \times e_{33}^* < 0$, suggests that Bain distortion had not been completed upon martensitic transformation; rather, a small part of the Bain strain remained as elastic strain in the martensite. The residual strain originating from Bain distortion is in good agreement with the experimental result that martensite had a small $c/a$, as indicated by macroscopic neutron diffractometry[1]. Indeed, when $c/a$ was estimated as $(1 + e_{33}^*)/(1 + e_{11}^*)$ with the above values of $e_{11}^* = -0.0018$ and $e_{33}^* = 0.0024$, the estimated value was 1.0042. This value is very close to the $c/a$ value evaluated by neutron diffractometry (1.0052). The relationship between the orientation distribution of tetragonally distorted bcc caused by the residual strain and the Bain groups in martensite will be discussed in the presentation.

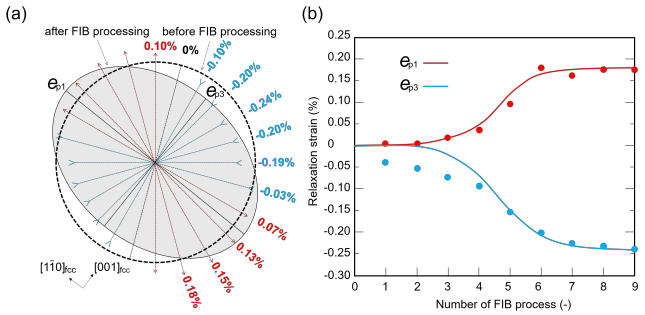


**Fig. 4**. The results of (a) the in-plane strain on the top surface of the micro-pillar, and (b) the development of the principal strains as a function of FIB processing step.

**3.3** Change in nanohardness by release of transformation induced internal stress

**Fig. 5** shows the load–displacement curve of IF martensite obtained by nanoindentation testing. It is known that the pop-in phenomenon[4] accompanied by discontinuous displacement occurs in nanoindentation testing due to the beginning of plastic deformation with an explosive increase in dislocations, but the IF martensite exhibited a continuous curve without pop-in. Other researchers have also reported that pop-in hardly occurs in martensite[5,6], which is because of the effect of mobile dislocations previously existing in martensite. Comparing the curves before and after the micropillar fabrication, it is found that the displacement clearly became larger after the micropillar fabrication at the load of 1000 μN, although the fabrication slightly reduced the displacement at early stage of nanoindentaiton. This means that the nanohardness markedly decreased with the micropillar fabrication. Taking into account the internal residual strain released by FIB processing, it can be concluded that the decrease in nanohardness was caused by the release of the internal residual strain.

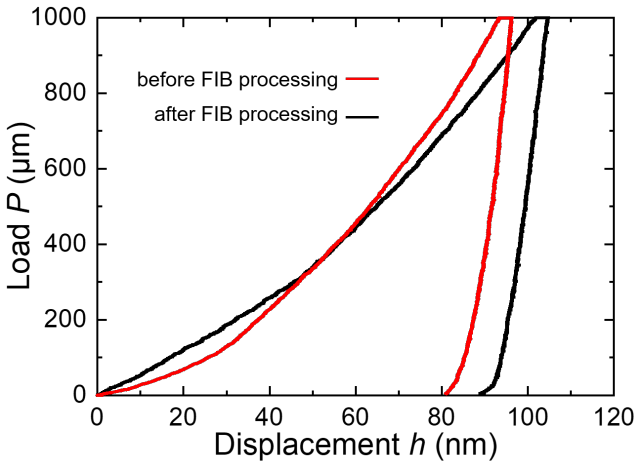


**Fig. 5**. Load-displacement curves of nano-indentation test in IF martensite before and after the micro-pillar fabrication.

## References


1) N. Maruyama, S. Tabata, and H. Kawata: Metall. Mater. Trans. A, **51** (2020) 1085-1097.
2) J. Lord, D. Cox, A. Ratzke, M. Sebastiani, A. Korsunsky, E. Salvati, M. Z. Mughal, and E. A. Bemporad: NPL Measurement Good Practice Guide, **143** (2018) 1-182.
3) F. Archie, M.Z. Mughal, M. Sebastiani, E. Bemporad, and S. Zaefferer: Acta Mater., **150** (2018) 327-338.
4) T. Ohmura, S. Matsuoka, K. Tanaka, and T. Yoshida: Thin Solid Films, **385** (2001) 198-204.
5) T. Ohmura, K. Tsuzaki, and S. Matsuoka: Scripta Mater., **45** (2001) 889-894.
6) L. Zhang, T. Ohmura, A. Shibata, and K. Tsuzaki: Mater. Sci. Eng. A, **527** (2010) 1869-1874.